

Dynamical mechanism of intrinsic localized modes in microelectromechanical oscillator arrays

Qingfei Chen,¹ Liang Huang,¹ Ying-Cheng Lai,^{1,2} and David Dietz³

¹*Department of Electrical Engineering, Arizona State University, Tempe, Arizona 85287, USA*

²*Department of Physics, Arizona State University, Tempe, Arizona 85287, USA*

³*Air Force Research Laboratory, Directed Energy Directorate, 3550 Aberdeen Ave. SE, Kirtland Air Force Base, New Mexico 87117, USA*

(Received 11 November 2008; accepted 15 January 2009; published online 13 March 2009)

Experimental evidence of intrinsic localized modes (ILMs) in microelectromechanical oscillator arrays has been reported recently. In this paper, we carry out a detailed analysis of a new mechanism for ILMs in typical experimental settings; that is, spatiotemporal chaos is ubiquitous and it provides a natural platform for actual realization of various ILMs through frequency control. We find that unstable periodic orbits associated with ILMs are pivotal for spatiotemporal chaos to arise and these orbits are the keys to stabilizing ILMs by frequency modulation. © 2009 American Institute of Physics. [DOI: [10.1063/1.3078706](https://doi.org/10.1063/1.3078706)]

Small-sized systems such as microelectromechanical (MEM) resonators have become common in many fields of science and engineering. These systems have a relatively simple structure but they show surprisingly rich nonlinear-dynamical behaviors such as bistability, chaos, and energy-localized oscillations. This paper focuses on intrinsic localized modes (ILMs) in MEM oscillator arrays. The phenomenon is characterized by the oscillations of a few oscillators with significantly larger amplitudes than the average amplitude. While ILMs have been identified in a wide variety of physical systems such as Josephson junctions, optical waveguide arrays, photonic crystals, and antiferromagnets, their discovery in MEM systems has been relatively recent. We shall report results from numerical computations and dynamical analysis of a generic class of MEM oscillator arrays, which suggest the fundamental role played by chaotic dynamics in generating ILMs. In particular, we find that spatiotemporal chaos provides a natural platform for ILMs. As MEM systems are employed extensively in device research and development, we expect our finding to be potentially useful.

I. INTRODUCTION

ILMs, also known as “discrete breathers” or “lattice solitons,” can occur in a defect-free nonlinear lattice, extending over only a few lattice sites.^{1–4} In basic physics, ILMs represent an interesting phenomenon as they are the result of purely nonlinear interactions. Theoretically, for conservative systems, the localized modes are exact solutions.^{5,6} In device applications, ILMs can be of significant concern as localized high-energy states can have undesirable effects on the operation of the device. ILMs have in fact been observed in many physical systems, such as Josephson junctions,⁷ optical waveguide arrays,⁸ photonic crystals,⁹ and antiferromagnets.¹⁰

Recently, ILMs have been discovered experimentally in MEM oscillator arrays.^{11,12} As such systems are the key com-

ponents in state-of-the-art technologies that are having ever increasing impacts on various areas of science and engineering,¹³ it is of considerable interest to explore the dynamical mechanism of ILMs in MEM oscillator arrays. The purpose of this paper is to offer a detailed analysis for the mechanism of ILMs in experimental systems. In particular, a route for exciting ILMs in MEM oscillator arrays through spatiotemporal chaos is presented.

While the dynamical mechanism of ILMs in conservative systems has been understood reasonably well,^{5,6} systems of MEM oscillator arrays are typically dissipative. Prior to our work, the status of understanding of ILMs in MEM oscillator arrays is as follows. It has been suggested that artificial impurities in MEM cantilever arrays can induce ILMs,¹⁴ and ILMs induced by a forced nonlinear vibration mode have also been realized.¹⁵ However, there is experimental evidence indicating that ILMs can be generated without any impurities.¹² In Ref. 16, besides ILMs, phenomena such as hopping and repulsion are reported, but the underlying mechanisms of these phenomena are not given. Computational study of MEM cantilever arrays of identical beam length has revealed that it is not possible to have modulational instability in the system, but ILMs can be generated by noise in combination with frequency chirping modulation.¹⁷ The conclusion appears to be that, in order for a MEM oscillator-array system to exhibit ILMs, the following two conditions are needed: (1) random heterogeneous initial conditions or noise and (2) modulation of driving frequency in time (frequency chirping).

The starting point of our analysis is a prototype system described by a set of coupled differential equations derived from experiments.¹¹ Since typical experimental settings to excite ILMs include the case where periodic forcing is applied to MEM arrays of alternating lengths, i.e., a long (short) beam has two short (long) beams as its nearest neighbors, one on each side,^{11,12} we will consider both the uniform-length and the alternating-length cases. The method of averaging can then be employed to reduce the system to a

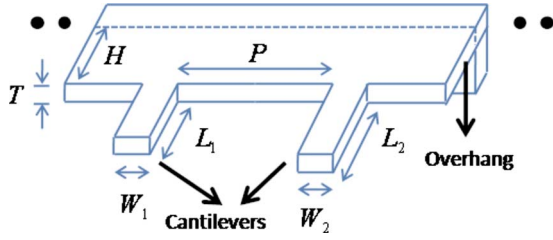


FIG. 1. (Color online) Schematic of a single cantilever unit in a typical experimental MEM array system, where $L_1, L_2, W_1, W_2, T, P,$ and H denote the beams' lengths, widths, thickness, length of the pitch, and length of the overhang, respectively.

form for which, in the zero-coupling limit, all possible equilibrium solutions can be obtained and their stabilities can be determined. Analytic continuation of the solutions into the finite-coupling regime reveals the coexistence of both locally high- and low-energy states (LESSs), which is a necessary condition for ILMs in MEM oscillator arrays. We find that, for the alternating-length case, spatiotemporal chaos can arise when the LES loses its stability, and ILMs can be excited naturally from chaos by frequency modulation, which can be abrupt with even uniform initial conditions for all oscillators in the absence of any external noise. A brief account of this phenomenon has been reported recently.¹⁸ In this paper, we carry out a detailed, systematic analysis of the dynamical mechanism for ILMs. Issues such as the existence of ILM states, their stabilities and bifurcations, the occurrence of spatiotemporal chaos, and the stabilization of ILMs from chaos by frequency modulation will be addressed.

In Sec. II, we describe the physics that leads to a generic model for MEM oscillator arrays, suitable for nonlinear-dynamics-based analysis. In Sec. III, the dynamics of ILMs are studied in detail. The mechanism for generating spatiotemporal chaos is investigated in Sec. IV, and the route to ILMs via chaos is demonstrated in Sec. V. Conclusions and discussion are presented in Sec. VI.

II. MODEL

The geometry of a single cantilever unit in a coupled MEM oscillator array employed in experimental studies¹² is shown in Fig. 1, where two cantilevers with alternating length are coupled by an overhang. The corresponding MEM array system can be fabricated by low-stress silicon nitride. Driving of the array is realized by a piezoelectric transducer. The material properties of the system are^{11,16} $L_1=50 \mu\text{m}$, $L_2=55 \mu\text{m}$, $W_1=W_2=15 \mu\text{m}$, $T=0.3 \mu\text{m}$, $H=23 \mu\text{m}$, and $P=40 \mu\text{m}$. The density and Young's modulus of the material are $\rho=2300 \text{ kg/m}^3$ and $E=110 \text{ GPa}$, respectively.

The dynamics of a MEM cantilever beam is in general described by a nonlinear partial differential equation¹⁹ that involves complicated mechanical and electrical interactions between the beam and its surroundings. For a single cantilever beam, the continuum equation of motion under driving force is¹¹

$$\rho A \frac{\partial^2 u}{\partial t^2} + EI \frac{\partial^4 u}{\partial s^4} + EI \frac{\partial}{\partial s} \left[\frac{\partial u}{\partial s} \frac{\partial}{\partial s} \left(\frac{\partial u}{\partial s} \frac{\partial^2 u}{\partial s^2} \right) \right] = \rho A \alpha \cos(\Omega t), \quad (1)$$

where $A=W \times T$ is the cross-sectional area of the beam and $I=(W \times T^3)/12$ is the moment of inertia. The displacement variable $u(s, t)$ can be expanded based on a set of orthonormal shape functions, denoted by $\phi_n(s)$, as follows:

$$u(s, t) = \sum_n \phi_n(s) \chi_n(t), \quad (2)$$

where $\chi_n(t)$ is the beam tip's displacement associated with ϕ_n . The shape functions satisfy the boundary conditions $\phi_n(0)=0$ and $\phi_n(L)=1$. Here, only the lowest frequency mode is kept. By substituting Eq. (2) into Eq. (1), multiplying $\phi_1(s)$ on both sides, and then integrating the equation over the length of the beam, one can obtain

$$m \frac{d^2 x(t)}{dt^2} + k_2 x(t) + k_4 x^3(t) = m \alpha \cos(\Omega t), \quad (3)$$

where $x(t)$ is the displacement of the beam's tip and $k_2=(12.36EI)/L^3$ and $k_4=(24.79EI)/L^5$ are the harmonic and the quadratic spring constants,¹¹ respectively. For coupled microcantilever arrays, the full dynamical equations are more complicated. The cantilevers are affected by their environment, generating various damping forces. They also interact with each other with coupling forces.

Without losing the essential dynamics of the system, we focus on the motions of the free ends of the beams, taking into account damping and coupling effects. The system equations can then be described by the following set of nonlinear ordinary differential equations:¹²

$$m_i \ddot{x}_i + b_i \dot{x}_i + k_{2i} x_i + k_{4i} x_i^3 + k_j (2x_i - x_{i+1} - x_{i-1}) = m_i \alpha \cos(2\pi f t), \quad (4)$$

where x_i ($i=1, \dots, N$) is the displacement of the end point of the i th cantilever beam of effective mass m_i , b_i is the damping coefficient, k_{2i} and k_{4i} are the on-site harmonic and quadratic spring constants of the i th beam, respectively, and k_j is the harmonic coupling spring constant which we choose as a bifurcation parameter of the system. Each beam is subject to a common sinusoidal driving characterized by acceleration α and frequency f . Let $\Omega=2\pi f$ and $x_i(t)=U_i(t)\cos(\Omega t) + V_i(t)\sin(\Omega t)$ and define $Q_i=\sqrt{m_i k_{2i}}/b_i$ and $\Omega_{0i}=\sqrt{k_{2i}/m_i}$ as the quality factor and the resonant frequency of beam i , respectively. When the driven frequency Ω is close to the resonant frequency and when the driving is strong, the beam dynamics can be strongly nonlinear, exhibiting a bistable response with either large- or small-amplitude oscillations. Moreover, in the bistable region, there exists an unstable solution between the two stable solutions.

We first consider the situation where all beams have identical length. The MEM array system equation (4) is in fact a system of coupled driven Duffing oscillators. The averaging technique^{20,25} can then be employed for moderate driven force. Let the averaged functions of $U_i(t)$ and $V_i(t)$ be $u_i(t)$ and $v_i(t)$, respectively. A straightforward averaging procedure leads to

$$\begin{aligned} \frac{du_i}{dt} &= -\frac{1}{2\Omega} \left[(\Omega^2 - \Omega_{0i}^2)v_i - \frac{3k_{4i}}{4m_i}v_i(u_i^2 + v_i^2) + \frac{\Omega_{0i}}{Q_i}\Omega u_i \right. \\ &\quad \left. - \frac{k_I}{m_i}(2v_i - v_{i+1} - v_{i-1}) \right], \\ \frac{dv_i}{dt} &= \frac{1}{2\Omega} \left[(\Omega^2 - \Omega_{0i}^2)u_i - \frac{3k_{4i}}{4m_i}u_i(u_i^2 + v_i^2) - \frac{\Omega_{0i}}{Q_i}\Omega v_i + \alpha \right. \\ &\quad \left. - \frac{k_I}{m_i}(2u_i - u_{i+1} - u_{i-1}) \right], \quad i = 1, \dots, N, \end{aligned} \tag{5}$$

which is in a form of a discrete nonlinear Schrodinger equation (NLSE)²⁰ driven by a constant force $\alpha/(2\Omega)$,

$$\begin{aligned} j\frac{d\xi_i}{dt} &= -\left[\frac{1}{2\Omega}(\Omega^2 - \Omega_{0i}^2) + j\frac{\Omega_{0i}}{2Q_i} \right] \xi_i + \frac{3}{8}\frac{k_{4i}}{\Omega m_i}|\xi_i|^2\xi_i - \frac{\alpha}{2\Omega} \\ &\quad + \frac{k_I}{2\Omega m_i}(2\xi_i - \xi_{i+1} - \xi_{i-1}) \end{aligned} \tag{6}$$

for $i=1, \dots, N$, where $\xi_i = u_i + jv_i$. For uniform beam length, Eq. (6) has a continuum limit. However, for the case of alternating beam length, Eq. (6) does not have the continuum limit and can only be analyzed as a coupled lattice system. Another difference between Eq. (6) and the standard coupled NLSE is that, for the latter, the coefficient of the first-order term on the right-hand side is complex.

III. DYNAMICS OF ILMs IN MEM OSCILLATOR ARRAYS

In this section, we systematically investigate the dynamics of ILMs in MEM oscillator arrays. We first study the dynamics of two coupled MEM oscillators and then extend the analysis to systems of larger numbers of oscillators.

A. Two coupled MEM oscillators

A key feature of ILMs is the coexistence of two groups of oscillators with high and low energies, respectively. To gain insight, we first study the case of two coupled oscillators. Although the case of coupled undamped NLSEs has been discussed in Ref. 21, to our knowledge, the driven damped NLSEs with complex coefficient which describe coupled MEM oscillator systems have not been studied. Here, we discuss the case of coupled beams of identical lengths.

Since Eq. (5) governs the evolution of the averaged motion, its equilibrium solutions correspond to oscillatory solutions of the actual system. A viable approach is to set $k_I=0$ to find all possible equilibrium solutions for the decoupled system and then analytically continue the solutions as k_I is increased from zero. Figures 2(a) and 2(b) show projections of the amplitudes of the averaged oscillations $A_1 = \sqrt{u_1^2 + v_1^2}$ and $A_2 = \sqrt{u_2^2 + v_2^2}$ versus k_I , respectively, where $A_1 > A_2$ (the case $A_2 > A_1$ is symmetrical). Parameters are chosen according to their corresponding experimental values:¹²

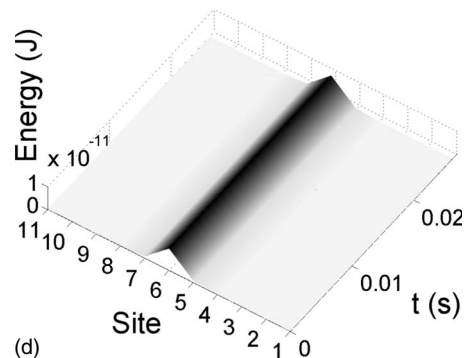
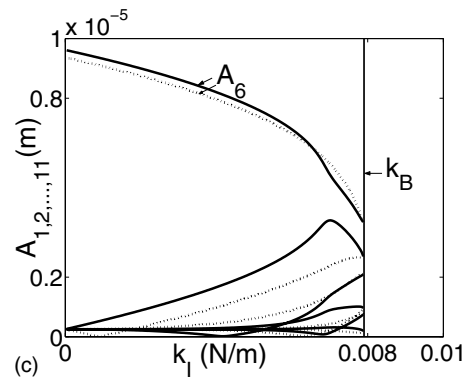
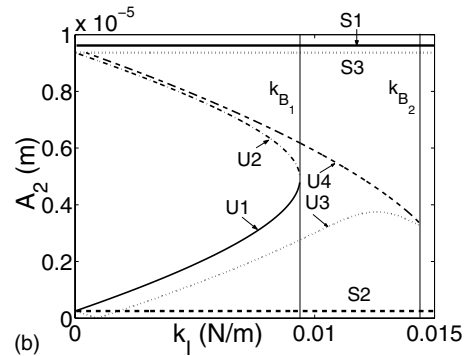
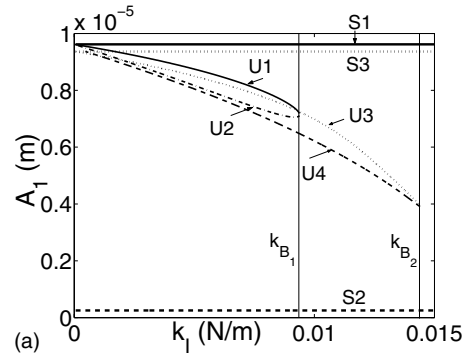


FIG. 2. Projections of solution locus: (a) $A_1 = \sqrt{u_1^2 + v_1^2}$ vs k_I and (b) $A_2 = \sqrt{u_2^2 + v_2^2}$ vs k_I for $N=2$. As k_I is decreased through the value denoted by the vertical line k_{B_1} , a S-N bifurcation occurs. The vertical line k_{B_2} denotes an unstable-unstable pair bifurcation. Oscillations of distinct amplitudes occur for $0 \leq k_I < k_{B_1}$. (c) For a system of $N=11$ beams, equilibrium solutions A_i vs the coupling parameter k_I . ILMs are possible for $0 < k_I < k_B \approx 0.008$ N/m. (d) A representative ILM state.

$$\begin{aligned} (m_i, b_i, k_{2i}, k_{4i}, f, \alpha) &= (5.46 \times 10^{-13} \text{ kg}, 6.24 \times 10^{-11} \text{ kg/s}, \\ &\quad 0.303 \text{ N/m}, 5 \times 10^8 \text{ N/m}^3, \\ &\quad 1.25 \times 10^5 \text{ Hz}, 1.56 \times 10^4 \text{ m/s}^2). \end{aligned}$$

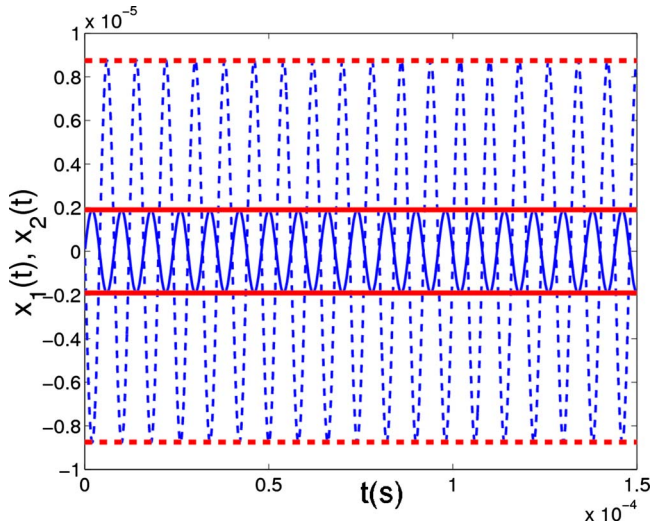


FIG. 3. (Color online) Time series $x_1(t)$ and $x_2(t)$ (thin solid and dashed traces) of unsynchronized solution U1 and their amplitudes obtained by the averaged model (thick horizontal solid and dashed lines) for $K_f=0.005$ N/m.

There are three synchronized solutions denoted by S1, S2, and S3 and four unsynchronized solutions labeled U1, U2, U3, and U4. The stable (unstable) solutions are represented by solid (dashed) lines. The vertical line denoted by k_{B_1} indicates a saddle-node (S-N) bifurcation point. We see that in the parameter region $k_f < k_{B_1}$, there is a stable equilibrium solution (U1) for which the oscillation amplitudes of the two beams are quite different, besides the existence of stable synchronized motions, which has the feature of ILM. To justify the use of the averaged system for approximating the driven system equation (4), we plot the time series $x_1(t)$ and $x_2(t)$ obtained directly from Eq. (4) (thin traces) and the amplitudes from the averaged system, as shown in Fig. 3 for $K_f=0.005$ N/m. We observe that the amplitudes of the time series agree with those from the averaged system very well.

We can now analyze the distinct dynamical states and their origins by focusing on the solutions in the decoupled limit (or anticontinuous limit) of Eq. (5) where $k_f=0$. A decoupled system can be transformed into polar coordinate as

$$\begin{aligned} \frac{dA_i}{dt} &= \frac{1}{2\Omega} \left[-\frac{\Omega\Omega_{0i}m_iA_i}{Q_i} - m_i\alpha \sin \theta_i \right], \\ \frac{d\theta_i}{dt} &= \frac{1}{2\Omega A_i} \left[(\Omega_{0i}^2 - \Omega^2)A_i + \frac{3k_4A_i^3}{4} - m_i\alpha \cos \theta_i \right], \end{aligned} \quad (7)$$

where $A_i = \sqrt{u_i^2 + v_i^2}$ and θ_i are the radial and angular coordinates of (u_i, v_i) (A_i and θ_i also denote the amplitude and the phase angle of x_i , respectively).

Consider the static solutions at the decoupled limit of system (5). There are in total three hyperbolic equilibria for each subsystem (7): $S_i^1 := \{(A_i, \theta_i) | A_i = M_1, \theta_i = T_1\}$, $S_i^2 := \{(A_i, \theta_i) | A_i = M_2, \theta_i = T_2\}$, and $S_i^3 := \{(A_i, \theta_i) | A_i = M_3, \theta_i = T_3\}$, where $i=1, 2$, $M_1=2.5218 \times 10^{-7}$ m, $M_2=9.6173 \times 10^{-6}$ m, $M_3=9.3655 \times 10^{-6}$ m, $T_1=1.0005\pi$, $T_2=-0.0176\pi$, and $T_3=-0.9828\pi$. For the case of $A_1 \geq A_2$, there are six solutions at the decoupled limit. In particular,

there are three homogeneous solutions (denoted as HOSs) where the dynamical states of the two oscillators are identical, that is,

$$\text{HOS1:}\{(A_1, \theta_1, A_2, \theta_2) | A_1 = M_1, \theta_1 = T_1, A_2 = M_1, \theta_2 = T_1\},$$

$$\text{HOS2:}\{(A_1, \theta_1, A_2, \theta_2) | A_1 = M_2, \theta_1 = T_2, A_2 = M_2, \theta_2 = T_2\},$$

and

$$\text{HOS3:}\{(A_1, \theta_1, A_2, \theta_2) | A_1 = M_3, \theta_1 = T_3, A_2 = M_3, \theta_2 = T_3\},$$

and three heterogeneous solutions (HESs),

$$\text{HES1:}\{(A_1, \theta_1, A_2, \theta_2) | A_1 = M_1, \theta_1 = T_1, A_2 = M_2, \theta_2 = T_2\},$$

$$\text{HES2:}\{(A_1, \theta_1, A_2, \theta_2) | A_1 = M_1, \theta_1 = T_1, A_2 = M_3, \theta_2 = T_3\},$$

and

$$\text{HES3:}\{(A_1, \theta_1, A_2, \theta_2) | A_1 = M_2, \theta_1 = T_2, A_2 = M_3, \theta_2 = T_3\}$$

(the other three HESs for $A_2 > A_1$ are considered to be the same as HES1, HES2, and HES3 due to symmetry). Among these solutions, HOS3, HES2, and HES3 are unstable since they have the unstable equilibrium S_i^3 in at least one of the two subsystems.

Since all the solutions at the decoupled limit are hyperbolic, when the value of k_f is continued from 0, the stabilities of the solutions can be maintained, as stipulated by the local stability theorem.²⁶ In Figs. 2(a) and 2(b), the solutions S2, S1, and S3 originate from HOS1, HOS2, and HOS3, respectively, and the solutions U1, U3, and U2 are extensions of HES1, HES2, and HES3, respectively. Since ILMs are spatially heterogeneous and are physically observable, they can only be continued from stable HESs. Therefore, among the solutions in Figs. 2(a) and 2(b), only U1 satisfies the condition and represents an ILM.

B. $N (>2)$ coupled MEM oscillators

We now treat the general case of $N > 2$. Following the same approach as for the $N=2$ case, we note that, in the bistable regime, a *single*, decoupled beam has three hyperbolic equilibria: two stable and one unstable. For $k_f=0$, there are 3^N hyperbolic equilibria. As these solutions are analytically continued from $k_f=0$, their number and stabilities remain the same, as guaranteed by the local stability theorem. There thus exists a finite parameter regime $k_f \geq 0$ in which each beam has two possible stable solutions: one of small and the other of large amplitude. An ILM corresponds to the situation where a few of the beams are in the large-amplitude state, while the remaining beams oscillate with small amplitudes. An examination of the basin structure of the single-beam dynamics reveals that the basin of the large-amplitude stable equilibrium is typically much smaller than that of the small-amplitude stable equilibrium. Thus, from random heterogeneous initial conditions, majority of the beams oscillate with small amplitude in the steady state while only a few may oscillate with relatively large amplitude. This indicates that, from the viewpoint of dynamics, ILMs are generic in the sense that the opposite situation where many more beams oscillate with large amplitude is typically unlikely. Physi-

cally, ILMs also represent collective motions of the system that are energetically favorable.

To illustrate how our analysis works, we present an example of finding an ILM for $N=11$, where the sixth beam oscillates with a high amplitude. In this case, we study the beam arrays with identical beam lengths and the parameters are set to be the same as the ones employed in Figs. 2(a) and 2(b). A solution for $k_I=0$ thus represents the state where this beam is initiated in the high-amplitude basin while the remaining ten beams are initially set to oscillate with low amplitude. Numerically obtained continuation of these solutions as k_I is increased from zero is shown in Fig. 2(c), where the vertical line at k_B denotes a S-N bifurcation point, beyond which only synchronized beam dynamics can occur. ILMs can be found for $0 < k_I < k_B \approx 0.008$ N/m. The spatiotemporal evolution of the beam energies is shown in Fig. 2(d) for $k_I=0.005$ N/m, where a spatially localized behavior in the energy can be seen.

While a stability analysis indicates that ILMs can arise typically in MEM oscillator arrays, it does not guarantee that ILMs can actually be observed in, for instance, a specific experiment. In previous works concerning MEM arrays with alternating beam lengths,^{12,16,17} it has been argued that, in order for ILMs to occur, (1) the initial state of the MEM beam system should be random to allow for spatial heterogeneity and (2) the frequency of the external driving should be increased gradually with time (frequency chirping) to enhance the heterogeneity. Our computations reveal, however, that both conditions can be relaxed. In particular, the degree of heterogeneity in the initial condition distribution can be made arbitrarily small. For instance, we can actually use null initial conditions for all beams. A new finding is that spatiotemporal chaos can occur typically in the parameter regime of low driving frequency due to the uneven distribution of the beam length, which can serve as the source of spatial heterogeneity for beam dynamics. Because of chaos, the required frequency chirping scheme can be replaced by a more abrupt frequency-changing scheme. Qualitatively, this can be seen by noting that chaos contains an infinite number of possibilities for dynamical state. Once the system is in a chaotic regime, a change in the driving frequency can stabilize the system in one of the ILM states. Depending on the amount of frequency change, different ILMs can be realized.

Figure 4 presents a space-time plot of the amplitudes of oscillating beams in the same system that has been used in previous experimental and numerical studies.¹² There are $N=256$ beams with alternating lengths. The parameters are¹²

$$(m_i, b_i, k_{2i}, k_{4i}) = (5.46 \times 10^{-13} \text{ kg}, 6.24 \times 10^{-11} \text{ kg/s}, 0.303 \text{ N/m}, 5 \times 10^8 \text{ N/m}^3)$$

for odd i , the long beams, and

$$(m_i, b_i, k_{2i}, k_{4i}) = (4.96 \times 10^{-13} \text{ kg}, 5.67 \times 10^{-11} \text{ kg/s}, 0.353 \text{ N/m}, 5 \times 10^8 \text{ N/m}^3)$$

for even i , the short beams. The initial displacements and velocities are all set to be zero. Figure 4 reveals a highly irregular behavior before $t_{\text{step}}=0.013$ s both in space and in time, which is characteristic of spatiotemporal chaos. At t_{step} ,

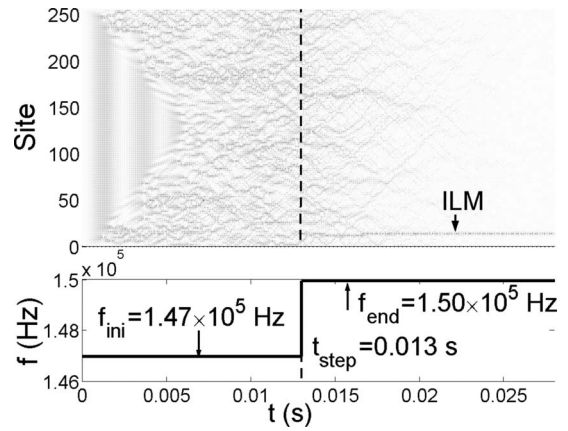


FIG. 4. Spatiotemporal chaos and ILM in a MEM oscillator array of $N=256$ beams for $k_I=0.0241$ N/m and $\alpha=1.56 \times 10^4$ m/s². The driving frequency is increased abruptly from 1.47×10^5 to 1.50×10^5 Hz at $t_{\text{step}}=0.013$ s.

the driving frequency is increased abruptly, generating an ILM about site 14. This result shows that with the heterogeneity associated with spatiotemporal chaos, ILMs can be generated in a noise-free system with uniform initial conditions.

IV. ORIGIN OF SPATIOTEMPORAL CHAOS

We consider systems of alternating lengths to demonstrate that spatiotemporal chaos is typical. Chaos plays the role of “internal noise” so that additional amplification as offered by frequency chirping is not necessary for the occurrence of ILMs. In this regard, we note that in the coupled NLSE, chaos has been found to be ubiquitous.^{22,23} In both the original MEM array system and the averaged system as described by the driven damped NLSE, we find that chaos is common. In fact, when the system size is not small (say, larger than a few coupled units), spatiotemporal chaos can arise. One example is shown in Fig. 4. Another example is shown in Fig. 5(a) for a system of $N=16$ coupled oscillators. The physical parameters and initial conditions are set to be the same as the ones used in Fig. 4 except for the smaller number of beams. The occurrence of chaos in the averaged system is exemplified in Fig. 5(b) in which the parameters and initial conditions of Fig. 5(a) are employed. Qualitatively, the spatiotemporal patterns in Figs. 5(a) and 5(b) are similar to each other, indicating that the averaged model equation (5) captures not only the static but also the dynamical behaviors of the original system equation (4). Since the averaged system is amenable to bifurcation analysis, we shall use it to explore the origin of spatiotemporal chaos.

A. Key bifurcations in the averaged model

In Figs. 2(a)–2(c), it is shown that the stable HESs disappear at certain bifurcation points in k_I . In the averaged model for the alternated-beam-length array system, there are two types of bifurcations leading to the destruction of some ILM state and the rise of LESs where all the beams oscillate with low amplitudes. These are the S-N and the stability-

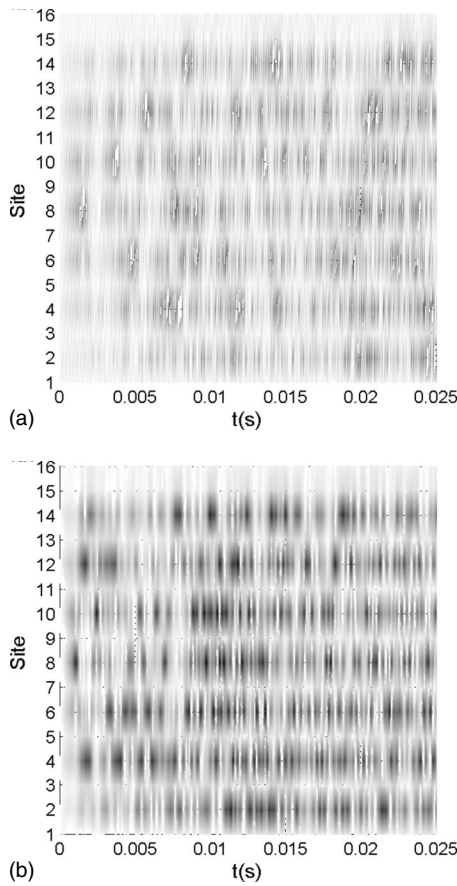


FIG. 5. (a) Spatiotemporal chaos in an original MEM array system of size $N=16$. (b) Spatiotemporal plot of A_i ($i=1,2,\dots,16$) in the corresponding averaged system (5).

transition (S-T) bifurcations, where the latter occurs when a stable fixed point loses its stability and becomes an unstable saddle.

In a MEM oscillator array, the destruction of ILMs and LESs can be attributed to the two types of bifurcations. Two examples for $N=16$ are presented in Fig. 6 where the stabilities of the particular solutions are determined by the sign of the largest eigenvalue of the Jacobian matrix in system (5). Figure 6(a) is a bifurcation diagram of an LES. It can be seen that the LES is destroyed when it collides with another unstable fixed point at the S-N bifurcation that occurs at $k_I \approx 0.0238$ N/m. The bifurcation diagram of an ILM is shown in Fig. 6(b), where the ILM becomes unstable for $k_I \geq 0.0234$ N/m. These bifurcations thus provide a base for understanding the occurrence of spatiotemporal chaos.

B. Occurrence of spatiotemporal chaos

Figure 7 shows a magnified bifurcation diagram combining Figs. 6(a) and 6(b). The two types of bifurcation divide the relevant parameter interval into three distinct regions. A LES exists in regions I and II, and it is destroyed by the S-N bifurcation that occurs at the value of k_I indicated by the right vertical line. In region I, an ILM fixed point also exists, and it becomes an unstable saddle at the value of K_I denoted by the left vertical line via an S-T bifurcation. Thus, in region I, there are two stable fixed points, one corresponding to

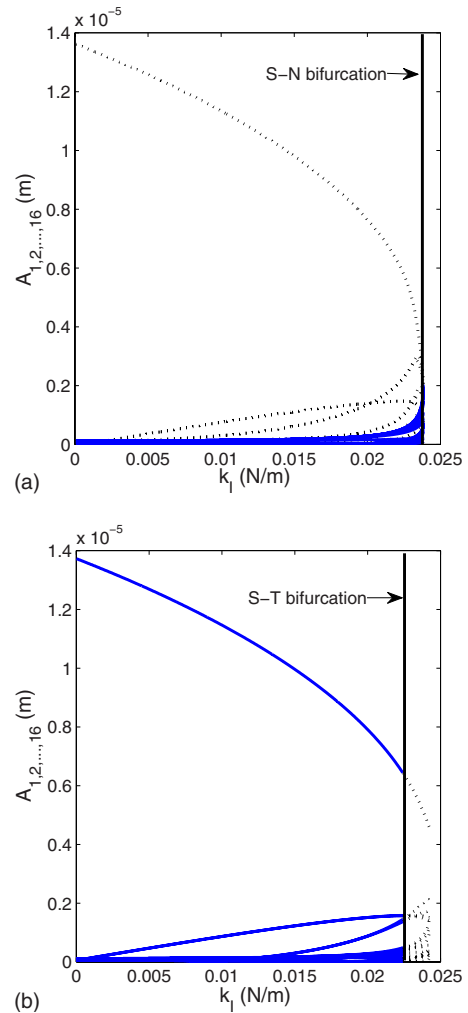


FIG. 6. (Color online) For the averaged system equation (5) of $N=16$ oscillators: (a) A S-N bifurcation for an LES and (b) an S-T bifurcation for an ILM.

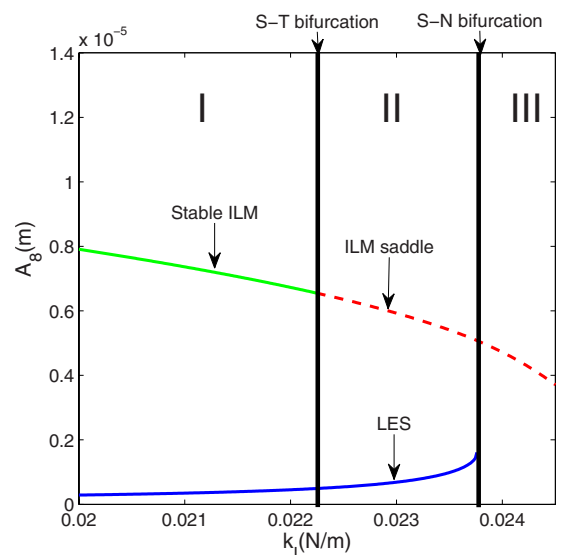


FIG. 7. (Color online) Typical bifurcation diagram of LES and ILM for the case of $N=16$.

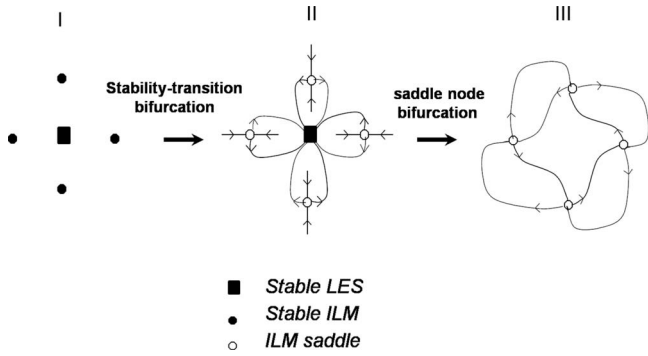


FIG. 8. Schematics of the dynamics in different regions of k_j .

the LES and another to ILM. In region II, only the LES is stable, and there are no stable fixed points in region III. Shown in Fig. 7 is a particular pair of ILM and LES solutions. Note that, in the full system, there are many pairs of such solutions.

A schematic illustration of the dynamics about these stable and unstable fixed points is shown in Fig. 8. In region I, the ILMs are denoted by solid circles and the LESs are denoted by solid squares. Because of the existence of multiple stable attractors (multistability), the phase space is divided according to the basins of attraction of these attractors. In region II, the ILMs are unstable but the LESs are still stable attractors. In region III, all orbits are unstable saddles, and their stable and unstable manifolds typically form a network of homoclinic and heteroclinic crossings, which generates horseshoe dynamics and henceforth chaos. The chaotic attractor thus contains all the unstable saddles as its skeleton, and a typical trajectory will visit the neighborhoods of the saddles alternately in time. Signatures of such saddles can be found in the space-time plot of the chaotic attractor, as shown in Fig. 9, where the ILM saddles are circled. When proper external perturbations are applied, some of the ILM saddles can be stabilized, generating stable, physically observable ILMs. As we will demonstrate next, frequency modulation is a natural means of such perturbation.

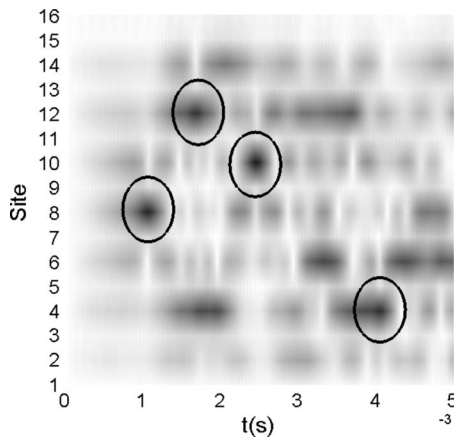


FIG. 9. Space-time plot of chaotic motion for $N=16$. Signatures of various ILM saddles are indicated by circles.

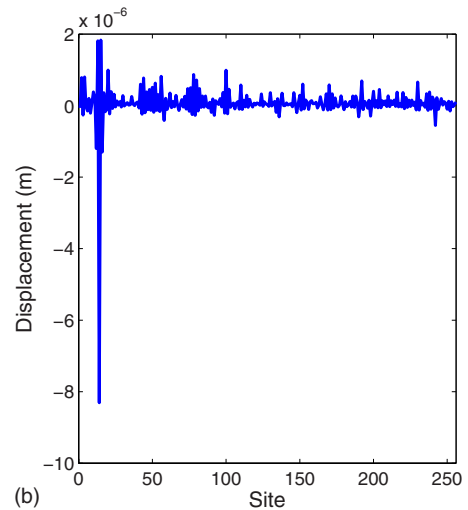
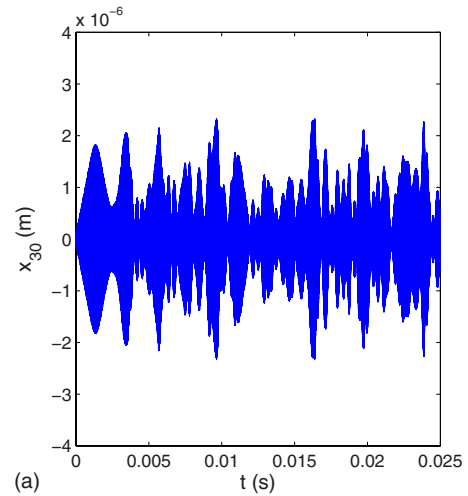


FIG. 10. (Color online) (a) Time series from spatial site 30 and (b) spatial profile at $t=0.0021$ s for a MEM oscillator-array system of size $N=256$.

V. ROUTE TO ILMs FROM SPATIOTEMPORAL CHAOS

Previous works have revealed that modulational instability is necessary to induce energy-localized motions in a nonlinear lattice.²⁴ This principle can also be applied to MEM oscillator-array system. In particular, we can set the system in a spatiotemporally chaotic state, a kind of modulational instability. Applying proper adjustments to the driving frequency can then stabilize the system about one of the ILMs. To obtain insight into the working of this mechanism, we plot in Figs. 10(a) and 10(b) a typical time series obtained at an arbitrary spatial site and a spatial plot at a fixed instant of time, respectively. It can be seen from Fig. 10(a) that there are bursts of the trajectory in various short time intervals, signifying modulational instability. A distinct feature of Fig. 10(b) is, however, a large spike at a certain spatial site. The intermittent bursts in the time series in Fig. 10(a) and the spatial spike in Fig. 10(b) suggest that the trajectory visits the neighborhoods of various ILM saddles. When the system trajectory moves near a particular ILM saddle, a perturbation in the form of sudden frequency change can stabilize the saddle. When this occurs, the system is likely to be in the basin of attraction of the corresponding stable ILM attractor

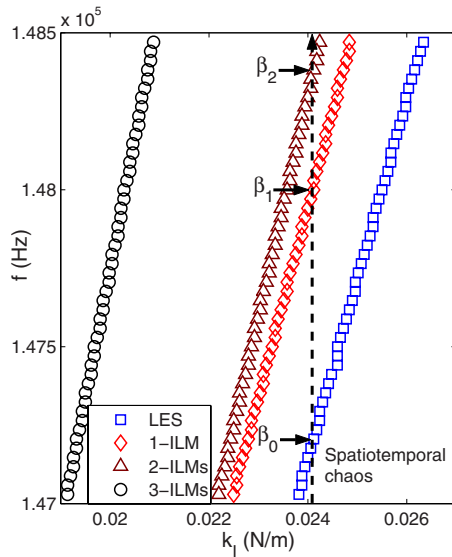


FIG. 11. (Color online) Boundaries between various asymptotic states including spatiotemporal chaos and various ILMs for a MEM system of $N=16$ beams in a two-dimensional, experimentally accessible parameter region.

since it is the continuation of the corresponding saddle. It is in this sense which we say that chaos provides a platform for generating ILMs through frequency modulation.

To further explore the chaos route to ILMs, it is useful to focus on the two-dimensional parameter space (k_1, f) , which is experimentally accessible. To facilitate testing of our predictions, we shall choose the ranges of the parameters as in typical experiments.^{11,12,16} Figure 11 shows, for a system of $N=16$ beams, boundaries between distinct asymptotic states including spatiotemporal chaos and various ILMs. In the figure, the region to the right of the “square” boundary is for spatiotemporal chaos and the region to the left denotes the state where the low-amplitude oscillation mode is stable but the high-energy mode is unstable (LES region); one ILM can be expected in the region to the left of the “diamond” boundary, two ILMs can occur in the region to the left of the “triangle” boundary, and so on. Figure 11 indicates that, for example, LESs and 1-ILM states are both possible in the parameter region in between the diamond and the triangle boundaries. For a given set of parameter values, distinct ILM states have different basins of attraction in the phase space. Now imagine an experimental situation where k_1 is fixed and the driving frequency is increased, as indicated by the vertical dashed line in Fig. 11 where $\beta_0, \beta_1,$ and β_2 are the intersections between the dashed line and the boundaries of the LES, 1-ILM, and 2-ILM regions, respectively. For $f < \beta_0$, the system has no stable equilibrium and it exhibits spatiotemporal chaos. For $\beta_0 < f < \beta_1$, there is one stable equilibrium in the averaged system, corresponding to stable oscillations of low oscillation energy state in the actual system. In this case, all initial conditions generate trajectories that approach the LES. For $\beta_1 < f < \beta_2$, both LESs and 1-ILM states are possible. That is, depending on the choice of initial conditions, all beams in the system can oscillate with low energy or the system can exhibit one ILM. For $\beta_2 < f < \beta_3$, the sys-

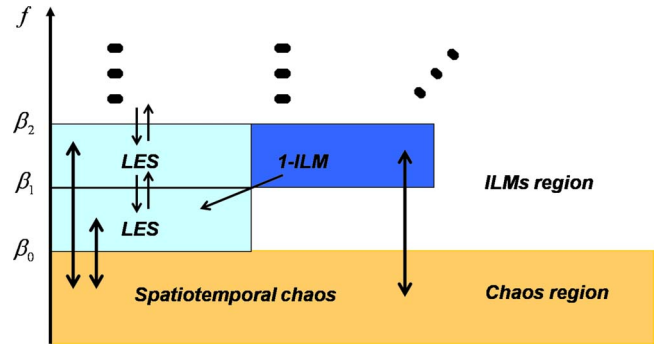


FIG. 12. (Color online) A schematic illustration of allowed and forbidden transitions between various states in a MEM oscillator array by frequency control.

tem can be in one of the three possible asymptotic states: LES, 1-ILM, and 2-ILM.

How does one physically realize ILMs? Focus, for instance, on the situation where the system exhibits one ILM. Figure 11 suggests one approach: initially set the system in spatiotemporal chaos by choosing a relatively small value of f and then increase the frequency to some value in between β_1 and β_2 . There is then a finite probability to drive the system into a 1-ILM state. Suppose now the frequency is reduced to some value in between β_0 and β_1 ; the system will then be in an LES. Equivalently, we say that there is a transition from a 1-ILM state to LES. A key point is that, it is practically impossible to change the system back into the 1-ILM state from the LES by increasing the frequency from some value in between β_0 and β_1 to some value in between β_1 and β_2 . The reason is that, once the system settles down in an LES, it will always be in its basin regardless of any frequency increase. In this sense, the transition from an LES directly to a 1-ILM state is forbidden. This line of reasoning suggests that, in the absence of any random factors, the only way to excite the system to a 1-ILM state is through spatiotemporal chaos. The same consideration applies to higher-order ILM states. For instance, a sufficient amount of frequency increase can bring the system from spatiotemporal chaos to a 2-ILM state. There can be transitions from a 2-ILM state to an LES or to a 1-ILM state, but the opposite transitions are not allowed. The possible transitions between various dynamical states are shown schematically in Fig. 12. The message is that, for a noiseless system, spatiotemporal chaos provides a natural platform for exciting ILMs in MEM oscillator arrays.

VI. CONCLUSION

We have carried out a nonlinear-dynamical-system analysis of the phenomenon of ILMs in MEM oscillator arrays. Utilizing the averaging method allows the origin of various oscillations, including ILMs, to be identified and their stabilities to be analyzed. In particular, the dynamical origin of spatiotemporal chaos is clarified in the averaged model. A bifurcation analysis then enables the scenarios for physically realizing various ILMs to be predicted. While previous works have emphasized that ILMs can occur without any defects in the system, some sort of random perturbation

is thought to be essential for experimentally observing ILMs in MEM oscillator arrays. Our study suggests that even this requirement can be relaxed. Insofar as the system is nonlinear, spatiotemporal chaos can arise, which contains all possible unstable modes; some of them are reminiscent of various ILMs as they become unstable (ILM saddle). These saddles can connect together as a heteroclinic network, inducing spatiotemporal chaos. Parameter modulations such as frequency control are therefore capable of “restoring” the ILMs from the corresponding ILM saddles. This dynamics-based view represents an alternative but more comprehensive approach to ILMs in coupled MEM oscillators, whose occurrence in physical systems has proven to be ubiquitous.

An implication of our results to experimental study of ILMs in MEM array systems is that the requirement of external noise can be relaxed. In particular, the experimental system in Ref. 12 employed bi-element beam arrays with perturbations (noise) to induce modulational instability and spatial heterogeneity, which are essential for creating ILMs. In MEM systems, it is generally nontrivial to generate spatially heterogeneous thermal noise and to use it to excite ILMs. It is thus desirable to search for an alternative mechanism to generate spatial heterogeneity required for ILMs. Our results have shown that, even in the absence of noise, modulational instability is possible with appropriate design of the system, such as using beams of alternating lengths. In fact, spatiotemporal chaos can serve effectively as a robust type of modulational instability, from which ILMs can be generated as a natural consequence of the collective dynamics of the system. External noise and amplification are not necessary for ILMs. We expect this finding to be useful for experimental study of ILMs in MEM array systems.

ACKNOWLEDGMENTS

This work was supported by AFOSR under Grant No. FA9550-06-1-0024.

- ¹S. A. Kiselev, S. R. Bickham, and A. J. Sievers, *Comments Condens. Matter Phys.* **17**, 135 (1995).
- ²P. G. Kevrekidis, K. Ø. Rasmussen, and A. R. Bishop, *Int. J. Mod. Phys. B* **15**, 2833 (2001).
- ³S. Flach and C. R. Willis, *Phys. Rep.* **295**, 181 (1998).
- ⁴R. Lai and A. J. Sievers, *Phys. Rep.* **314**, 147 (1999).
- ⁵S. Aubry, *Physica D* **103**, 201 (1997).
- ⁶R. S. MacKay and S. Aubry, *Nonlinearity* **7**, 1623 (1994).
- ⁷P. Binder, D. Abraimov, A. V. Ustinov, S. Flach, and Y. Zolotaryuk, *Phys. Rev. Lett.* **84**, 745 (2000).
- ⁸R. Morandotti, U. Peschel, J. S. Aitchison, H. S. Eisenberg, and Y. Silberberg, *Phys. Rev. Lett.* **83**, 2726 (1999).
- ⁹S. F. Mingaleev and Y. S. Kivshar, *Phys. Rev. Lett.* **86**, 5474 (2001).
- ¹⁰M. Sato and A. J. Sievers, *Nature (London)* **432**, 486 (2004).
- ¹¹M. Sato, B. E. Hubbard, and A. J. Sievers, *Rev. Mod. Phys.* **78**, 137 (2006).
- ¹²M. Sato, B. E. Hubbard, A. J. Sievers, B. Ilic, D. A. Czaplewski, and H. G. Craighead, *Phys. Rev. Lett.* **90**, 044102 (2003).
- ¹³*Classical and Seminar Papers to 1990*, edited by W. S. Trimmer (IEEE, New York, NY, 1997).
- ¹⁴M. Sato, B. E. Hubbard, A. J. Sievers, B. Ilic, and H. G. Craighead, *Europhys. Lett.* **66**, 318 (2004).
- ¹⁵A. J. Dick, B. Balachandran, and C. D. Mote, Jr., *Proc. SPIE* **6166**, 61660N (2006).
- ¹⁶M. Sato, B. E. Hubbard, L. Q. English, A. J. Sievers, B. Ilic, D. A. Czaplewski, and H. G. Craighead, *Chaos* **13**, 702 (2003).
- ¹⁷P. Maniadis and S. Flach, *Europhys. Lett.* **74**, 452 (2006).
- ¹⁸Q. Chen, L. Huang, and Y.-C. Lai, *Appl. Phys. Lett.* **92**, 241914 (2008).
- ¹⁹S. K. De and N. R. Aluru, *Phys. Rev. Lett.* **94**, 204101 (2005); *J. Microelectromech. Syst.* **15**, 355 (2006).
- ²⁰Y. S. Kivshar and M. Peyrard, *Phys. Rev. A* **46**, 3198 (1992).
- ²¹J. C. Eilbeck, P. S. Lomdahl, and A. C. Scott, *Physica D* **16**, 318 (1985).
- ²²M. J. Ablowitz, B. M. Herbst, and C. M. Schober, *Physica A* **228**, 189 (1996).
- ²³E. Shlizerman and V. Rom-Kedar, *Phys. Rev. Lett.* **96**, 024104 (2006).
- ²⁴I. Daumont, T. Dauxois, and M. Peyrard, *Nonlinearity* **10**, 617 (1997).
- ²⁵J. Guckenheimer and P. Holmes, *Nonlinear Oscillations, Dynamical Systems, and Bifurcations of Vector Fields* (Springer, New York, 1983).
- ²⁶E. Groesen and E. Jager, *Studies in Mathematical Physics* (Elsevier Science, Amsterdam, The Netherlands, 1991), Vol. 2.